Applied Surface Science 285P (2013) 431–439

Contents lists available at ScienceDirect

Applied Surface Science

journal homepage: www.elsevier.com/locate/apsusc

Chemical and structural properties of polymorphous silicon thin films grown from dichlorosilane

C. Álvarez-Macías [a], B.M. Monroy [a], L. Huerta [a], M.A. Canseco-Martínez [a], M. Picquart [b], J. Santoyo-Salazar [c], M.F. García Sánchez [d], G. Santana [a,*]

[a] Instituto de Investigaciones en Materiales, Universidad Nacional Autónoma de México, A.P. 70-360, Coyoacán, C.P. 04510 México, D.F., Mexico
[b] Departamento de Física, Universidad Autónoma Metropolitana, Iztapalapa, A.P. 55-534, 09340 México, D.F., Mexico
[c] Departamento de Física, CINVESTAV-IPN, A.P. 14-740, C.P. 07000 México, D.F., Mexico
[d] Unidad Profesional Interdisciplinaria en Ingeniería y Tecnologías Avanzadas, Instituto Politécnico Nacional, Av. I.P.N. 2580, Gustavo A. Madero, 07340 México .D.F., Mexico

ARTICLE INFO

Article history:
Received 12 February 2013
Received in revised form 16 July 2013
Accepted 18 August 2013
Available online 26 August 2013

Keywords:
Polymorphous silicon
Dichlorosilane
PECVD
Nanocrystals
AFM
Raman
XPS
FTIR

ABSTRACT

We have examined the effects of hydrogen dilution (R_H) and deposition pressure on the morphological, structural and chemical properties of polymorphous silicon thin films (pm-Si:H), using dichlorosilane as silicon precursor in the plasma enhanced chemical vapor deposition (PECVD) process. The use of silicon chlorinated precursors enhances the crystallization process in as grown pm-Si:H samples, obtaining crystalline fractions from Raman spectra in the range of 65–95%. Atomic Force Microscopy results show the morphological differences obtained when the chlorine chemistry dominates the growth process and when the plasma–surface interactions become more prominent. Augmenting R_H causes a considerable reduction in both roughness and topography, demonstrating an enhancement of ion bombardment and attack of the growing surface. X-ray Photoelectron Spectroscopy results show that, after ambient exposure, there is low concentration of oxygen inside the films grown at low R_H, present in the form of Si—O, which can be considered as structural defects. Instead, oxidation increases with deposition pressure and dilution, along with film porosity, generating a secondary SiO_x phase. For higher pressure and dilution, the amount of chlorine incorporated to the film decreases congruently with HCl chlorine extraction processes involving atomic hydrogen interactions with the surface. In all cases, weak silicon hydride (Si—H) bonds were not detected by infrared spectroscopy, while bonding configurations associated to the silicon nanocrystal surface were clearly observed. Since these films are generally used in photovoltaic devices, analyzing their chemical and structural properties such as oxygen incorporation to the films, along with chlorine and hydrogen, is fundamental in order to understand and optimize their electrical and optical properties.

© 2013 Elsevier B.V. All rights reserved.

1. Introduction

Hydrogenated polymorphous silicon (pm-Si:H) consists in different silicon crystalline phases (nanocrystals, microcrystals, etc.) embedded in an hydrogenated amorphous silicon (a-Si:H) matrix. Due to its specific nanostructure pm-Si:H is a suitable candidate for application in silicon-based thin film solar cells because, despite being heterogeneous, it exhibits improved electronic transport and stability properties compared to those of a-Si:H [1–3]. Typically, pm-Si:H films have been deposited by plasma enhanced chemical vapor deposition (PECVD) using highly diluted silane (as precursor gas) in hydrogen mixtures. The effect of the plasma deposition parameters (such as the chamber pressure and dilutions $H_2/SiH_4 + H_2$) on the structural, electric, and optical properties has been previously studied [3–7]. However, the use of high hydrogen dilutions can contribute to an excessive incorporation of weak Si—H bonds into the pm-Si, resulting unsuitable for thin-film, photovoltaic applications [8–10]. For this reason, alternative passivating atoms with higher mass and lower diffusion coefficient than hydrogen, such as deuterium, fluorine and chlorine, are being investigated [11,12]. Chlorinated silanes, i.e., SiH_2Cl_2, $SiHCl_3$ and $SiCl_4$ have been used aiming at the improvement of material properties [13–15]. These studies have focused on the growth of epitaxial silicon by thermal CVD at high temperatures and low pressures. They discuss the layer-by-layer growth mechanism in terms of the passivating role of chlorine on the silicon surface. Also, the details of chlorine extraction by hydrogen are discussed.

* Corresponding author at: Departamento de Materia Condensada y Criogenia, Instituto de Investigaciones en Materiales, UNAM, Circuito Exterior s/n, C.U., A.P. 70-360, Coyoacán, 04510 México D.F., Mexico. Tel.: +52 55 56224722.
E-mail addresses: gsantana@iim.unam.mx, gsantana1963@yahoo.com.mx (G. Santana).

0169-4332/$ – see front matter © 2013 Elsevier B.V. All rights reserved.
http://dx.doi.org/10.1016/j.apsusc.2013.08.073

Table 1
Growth conditions of pm-Si:H thin films deposited by PECVD.

Power = 150 W, Ar flow = 50 sccm, SiH_2Cl_2 flow = 5 sccm		
$T_{substrate}$ = 200 °C, growth time = 30 min		
Chamber pressure (mTorr)	Hydrogen flow (sccm)	Hydrogen dilution ratio, R_H $H_2/(SiH_2Cl_2 + H_2)$
250 and 500	25	83.3
	50	90.9
	75	93.8
	100	95.2

However, in PECVD processes two important differences are present: both atomic hydrogen and chlorine precursors are activated in the discharge and plasma–surface interactions are important in determining the film growth mechanism [9,10,16–18].

The use of chlorine in PECVD processes has some advantages such as (i) improved crystallization in as grown samples, (ii) use of lower substrate temperatures and (iii) smaller incorporation of weak Si—H bonds. Recently, using dichlorosilane (SiH_2Cl_2) we have obtained different crystalline silicon formations (nc-Si to μc-Si) inside of the amorphous matrix, depending on the deposition conditions [19–23]. However, more extensive studies about the effects of chlorine chemistry in plasma systems are needed. For example, morphology analysis can help to infer the effects of different regimes of plasma–surface interactions (growth or attack), which depend on the plasma chemistry. Also, the limits in which chlorine incorporation to the films influences the degradation of their properties remain to be studied in more detail.

In this work we examined the effects of deposition pressure and hydrogen dilution ratio on surface roughness, crystalline volume fractions and chemical stability of pm-Si:H thin films, deposited by PECVD using dichlorosilane. We analyze the correlations between deposition conditions, chemical composition and their influence on the nanocrystals formation; nanocrystals surface passivation, oxidation level and porosity of the films.

2. Experimental

Pm-Si:H thin films were grown in a conventional PECVD system with parallel plates of 150 cm^2 and 1.5 cm apart, activated by a RF signal of 13.56 MHz [19–23]. Depositions were performed at pressures of 250 and 500 mTorr and H_2 flow rates of 25, 50, 75 and 100 sccm, keeping the other parameters constant. Growth conditions are summarized in Table 1. Films were deposited simultaneously on high resistivity (around 200 Ω cm) crystalline silicon (1 0 0) and quartz substrates, for infrared spectroscopy and Raman characterizations, respectively. Before the deposition, substrates were subjected to cleanup following a standard procedure [19,21].

Surface analysis was performed in an atomic force microscope (AFM), JEOL JSPM4210. The images were processed with Win SPM Processing Analysis software, version 2.00. Film thickness and growth rates were determined with a Sloan Dektak IIA profilometer and corroborated by Scanning Electron Microscopy (SEM) in a Carl Zeiss Auriga field emission microscope Micrographs were obtained with the secondary electron and in-lens detectors. Nanostructural analysis was performed using a Raman equipment model T64000 with Horiba Jobin-Yvon triple monochromator. The excitation source was an Ar+ Lexcel laser of 514.5 nm. All measurements were performed at room temperature in air. The samples were irradiated at a power of 20 mW in a spot size around 1 mm^2 to prevent laser-induced crystallization. The measuring range was between 400 and 600 cm^{-1}, the integration time of measurements was 1 min and the Raman signal was acquired by a cooled CCD detector. The atomic compositions were obtained by X-ray Photoelectron Spectroscopy (XPS) analysis in a VG Microtech Multilab ESCA 2000 system, equipped with a hemispherical-multichannel detector CLAM4-MDC, in which we determined the presence of Cl and O in the samples, as well as the chemical oxidation state of Si. XPS analysis was performed on the films grown over silicon substrates. The spectra were obtained using the MgKα ($h\nu$ = 1253.6 eV) X-ray source, operated at 15 kV and 20 mA. Erosion of the surface was performed using Ar^+ ions in vacuum to obtain composition profiles. The erosion rate was approximately 6.5 nm/min. Fourier transform infrared (FTIR) spectra of the films were recorded in transmittance mode using a Nicolet-210 FTIR spectrometer in the range 400–4000 cm^{-1}.

3. Results and discussion

3.1. Atomic force microscopy

Fig. 1 shows typical AFM 3D micrographs of pm-Si:H films deposited on crystalline silicon (1 0 0), which were grown at 250 mTorr with different hydrogen dilutions (R_H) of 83.3, 90.9, 93.8 and 95.2, respectively. Comparing images (a–d), important changes on the surfaces topography are observed with increasing hydrogen dilution. When R_H goes from 83.3 to 90.9 the shape of the clusters changed drastically from elongated to round. Also, the density of clusters is higher. When R_H goes from 90.9 to 93.8, no changes are observed in the density, but the morphology becomes elongated again (as in Fig. 1a). Finally, when R_H goes from 93.8 to 95.2 the size of clusters increases slightly but the density is maintained.

Fig. 2a shows the height distributions derived from the previous topographic images of pm-Si:H as a function of R_H (represented by color). The mean square roughness (RMS) is included for each case. We can see that, except for the sample grown with the lowest hydrogen dilution, the films present a broad and asymmetric height distribution. The peak of the distribution indicates the mean cluster height. It is notable that the sample with R_H = 83.3 has the narrowest height distribution with the smallest height. Moreover, this sample shows the minimum value of RMS (1.32 nm). This indicates that the surface of this film is the smoothest of all grown at 250 mTorr. On the other hand, at R_H = 90.9 a pronounced increase in RMS is observed from 1.32 nm to 5.38 nm. Also, a wider height distribution and increased average height are obtained. This is consistent with the clusters formation analyzed in Fig. 1. When R_H is increased from 90.9 to 95.4, appreciable RMS changes are not observed; but the peak of the distribution had a shift to minor heights when dilution is increased from 90.9 to 95.4.

Fig. 3 shows the AFM micrographs of the samples grown at 500 mTorr with R_H of 83.3, 90.9, 93.8 and 95.2. Analysis of images (a–d) shows that the surface morphology is modified with increasing hydrogen dilution. When R_H goes from 83.3 to 90.9 the clusters were decreased both in size and in height, showing a less elongated shape. In Fig. 3c and d, when R_H increases, this trend continues culminating in clusters of round shape. Fig. 2b shows the corresponding height distributions and different RMS roughness as a function of R_H. When R_H is increased from 83.3 to 90.9, there was a considerable reduction in both roughness and topography, which go from 13.6 nm to 2.9 nm and from 50 nm to 10 nm, respectively. From the height distribution and RMS trends, one can perceive that the topography becomes smoother with increasing hydrogen dilution. It can be noted that with the increase in deposition pressure, the surface morphology presents a different trend with increasing hydrogen dilution than the one observed in Figs. 1 and 2a.

Since the substrate temperature was the same in all cases (200 °C), we assume that the mobility of precursor species in the growth surface activated by thermal means is similar for all these films. Therefore, the morphological differences that can be observed in the AFM micrographs are mainly related to the

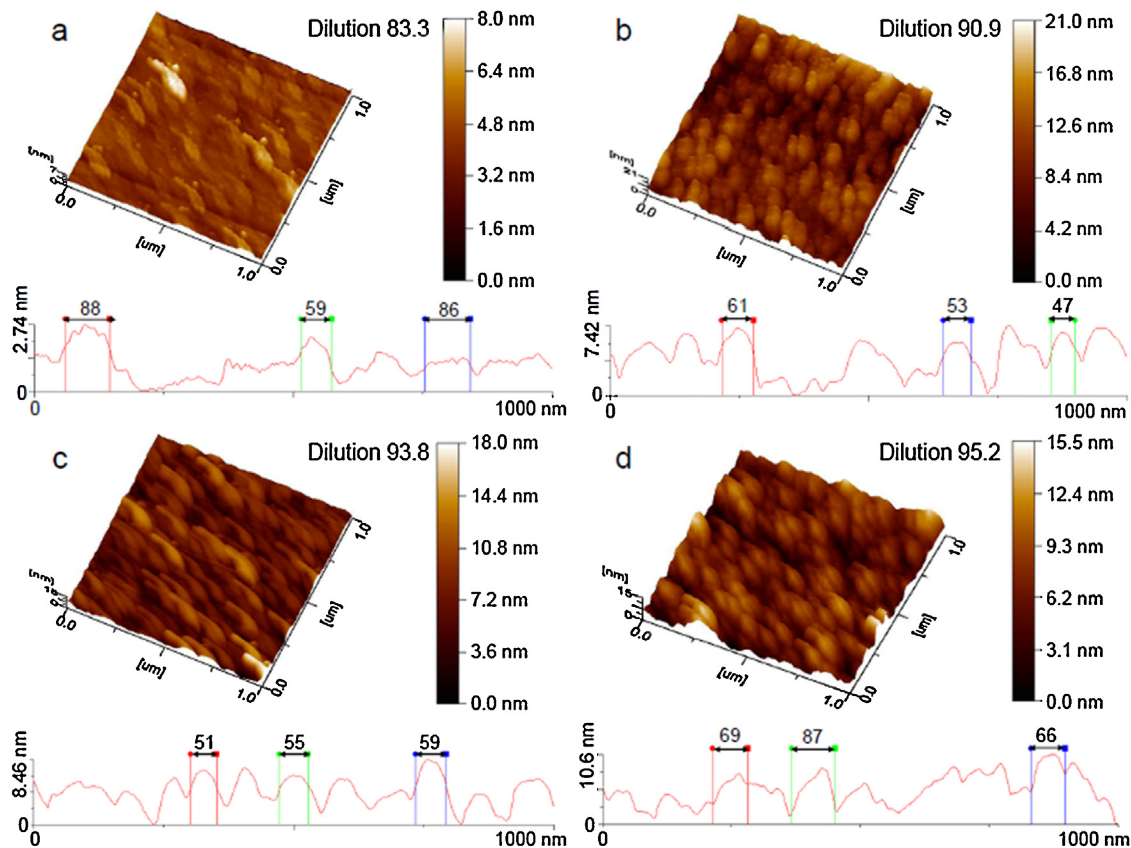

Fig. 1. 3D topography of pm-Si:H films grown by PECVD at 250 mTorr with dilution of: (a) 83.3, (b) 90.9, (c) 93.8 and (d) 95.2.

plasma–surface interactions. Augmenting the deposition pressure causes the mean free path of gas species to diminish. This implies that the residence time of species inside the plasma is greater and the decomposition of gas precursors is more efficient. On the other hand, incrementing hydrogen dilution promotes interactions of atomic H and Si—H and Si—Cl bonds that result in higher density of nucleation sites, increased chlorine extraction from the film, an increased silicon coverage, but also an enhancement of ion bombardment and attack of the growing surface [2,9,17,18]. Therefore, for the sample grown at smaller pressure and low dilution, the role of chlorine on the surface morphology is more prominent. Chlorine as a passivating atom of silicon surfaces has been studied before in epitaxial growth regimes [13–15]. Chlorine atoms act as terminal bonds and a smoother surface is expected with grains of low height as the ones presented in Fig. 1a. The trend for higher dilutions is dominated by the creation of nucleation sites that increment the grain density and decreases their average height. At 500 mTorr there is an increase in the amount of atomic hydrogen that impinges on the film surface generating a morphological change. The attack of the surface increases with higher dilutions causing grain fragmentation as evidenced in Fig. 4. Several authors have shown there is a strong correlation between the degree of H- and Cl-termination and the roughness at the growing surface, as well as in the structure [18,24,25].

Growth rates are reported in Table 2. As we have shown before, based on the morphology analysis, there is a change between growth and attack regimes that depends strongly on hydrogen dilution and deposition pressure. These parameters have a direct incidence on the ion bombardment of the surface. Therefore, a linear relationship between growth rate and hydrogen dilution is not observed, neither with the deposition pressure. The deposition rate was between 7 and 12 nm/min. In general, the growth rate increases with hydrogen dilution, but it decreases with increasing deposition pressure. This is consistent with an increased ion bombardment of the growing surface when pressure is augmented.

3.2. Raman spectroscopy

Fig. 5 shows the Raman spectra for all the deposited pm-Si:H thin films. The spectra show two vertical lines associated to the silicon transverse optical mode at 520 cm^{-1}, which is attributed to the crystalline phase, and at 480 cm^{-1}, attributed to the amorphous phase [9,24–28]. For samples grown at 250 mTorr, the Raman peak sharpens and there is a shift of the peak position toward 520 cm^{-1} at higher dilutions. The trend changes at 500 mTorr. Initially, for low R_H values (83.3 and 90.9) broad peaks are obtained. Then, at $R_H = 93.8$ a sharp peak is observed which broadens and shifts to lower wavenumbers with the increase to 95.2. Several authors have shown that the asymmetries located between 500 and 519 cm^{-1} are associated to the existence of a nanocrystalline phase [22–24,28].

Each spectrum shown in Fig. 5 was deconvoluted following the next criteria: two Lorentzian curves, corresponding to nano and microcrystalline contributions, and a Gaussian curve corresponding to the amorphous phase [22–24,28]. The peaks of the amorphous and microcrystalline phases are fixed at 480 cm^{-1} and 520 cm^{-1}, respectively. The third peak, associated to the nanocrystalline phase, is located at the best fit between 500 and 519 cm^{-1}. We obtained the crystalline volume fraction, X_C, using relation 1. The area of the curves are designated as I_A, I_N, and I_C, for the peaks of amorphous, nanocrystalline and microcrystalline phases, respectively [9,24–28].

$$X_C = \frac{I_N + I_C}{I_N + I_C + I_A} \quad (1)$$

Table 2
Crystalline volume fraction, average crystallite size and growth rate of pm-Si:H samples.

Pressure (mTorr)	Hydrogen dilution R_H	Average crystallite size D_R (nm)	Crystalline volume fraction X_C (%)	Growth rate (nm/min)
250	83.3	2.7	70	9.1
	90.9	2.4	83	10.8
	93.8	3.2	69	10.1
	95.2	4.2	94	11.8
500	83.3	2.8	92	7.8
	90.9	3.1	65	8.2
	93.8	3.3	95	9.4
	95.2	3.4	94	10.4

We calculated the mean grain size, D_R, using relation 2 based on the quantum confinement model where $\Delta\nu$ is the frequency peak shift of the nanocrystalline phase with respect to 520 cm^{-1} [9,24–28].

$$D_R = 2\pi\sqrt{\frac{2.24}{\Delta\nu}} \quad (2)$$

These results are reported in Table 2.

An important difference of these materials with respect to films obtained using silane as precursor is that we can obtain crystalline fractions exceeding 60% as grown. Changing deposition conditions we get X_C from 65% to 95%. From the Raman spectra we can observe that the nanocrystalline phase is prominent in all samples.

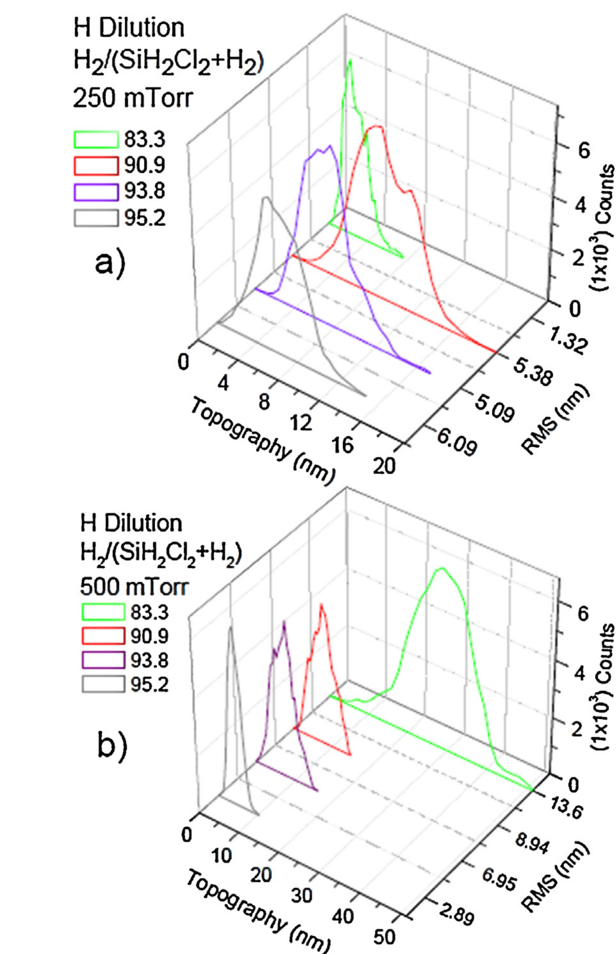

Fig. 2. RMS roughness and topography height distribution of pm-Si:H films grown at (a) 250 mTorr and (b) 500 mTorr, as a function of hydrogen dilution represented in color. (For interpretation of the references to color in this figure legend, the reader is referred to the web version of the article.)

At 250 mTorr, D_R is between 2.7 nm and 4.2 nm. At 500 mTorr, the average crystallite size is around 3 nm.

All samples were grown at a substrate temperature of 200 °C, which is in the threshold of amorphous to crystalline transition, not enough to produce 65–90% crystallinity as observed in our as grown samples. Therefore, we believe that the plasma–surface interactions changed by hydrogen dilution and deposition pressure are the main factors for the induced crystallinity during growth. Therefore, the high films' crystallinity observed in this work can be related to the chlorine chemistry introduced in the PECVD process which allows the use of low hydrogen dilutions and pressures during growth. In contrast, for samples deposited with SiH_4, high plasma densities or high hydrogen dilutions are needed to obtain similar crystalline fractions [29].

In the SiH_2Cl_2 system, when SiH_xCl_y $(x+y<3)$ impinges on the growing surface, both hydrogen and chlorine are preferentially extracted as HCl and bring forth the film deposition. The exothermic reaction of atomic hydrogen with chlorine releases a considerable amount of energy, sufficient to promote local crystallization [2,20–23]. Another consequence of this reaction is that less bonded hydrogen remains in the films.

3.3. X-ray photoelectron spectroscopy

Fig. 6 shows the chemical composition profiles of all samples. The atomic percents corresponding to Cl, O and Si are reported, because hydrogen is not detectable by this technique. Different depths of the sample were probed by sputtering the surface with argon ions for different erosion times in vacuum. The films are mainly composed by silicon (squares). However, important concentrations of oxygen (triangles) are detected in some samples. The amount of chlorine (circles) is always lower than 10%. It is possible to observe that Si and O concentrations changed with erosion time. In the film surface (0 s of erosion time) oxygen concentrations around 50% are detected in all samples. This value decreases to less than 15% with erosion time, except in some samples with elevated R_H where oxygen concentration remains above 25% for all erosion times.

It is important to note that oxygen is absent from the deposition process, thus oxygen detected by XPS is due to posterior oxidation of the samples. Surface oxidation is always expected in silicon thin films. This is observed in the high oxygen concentration at low erosion times in all samples. For the samples grown at higher R_H, oxidation can be observed throughout the film thickness. This effect is more pronounced for the series deposited at 500 mTorr. Since these are all as grown films, not subjected to any kind of thermal annealing, these films must have a porous structure inside to present an oxidation process due to hydrolysis reactions with ambient exposure [8]. The porosity of these films was observed by cross section SEM images (Fig. 7). As explained before, for high pressure and high hydrogen dilutions, atomic hydrogen tends to attack the growth surface increasing the defects density and enhancing the number of voids, as evidenced in the morphological study by

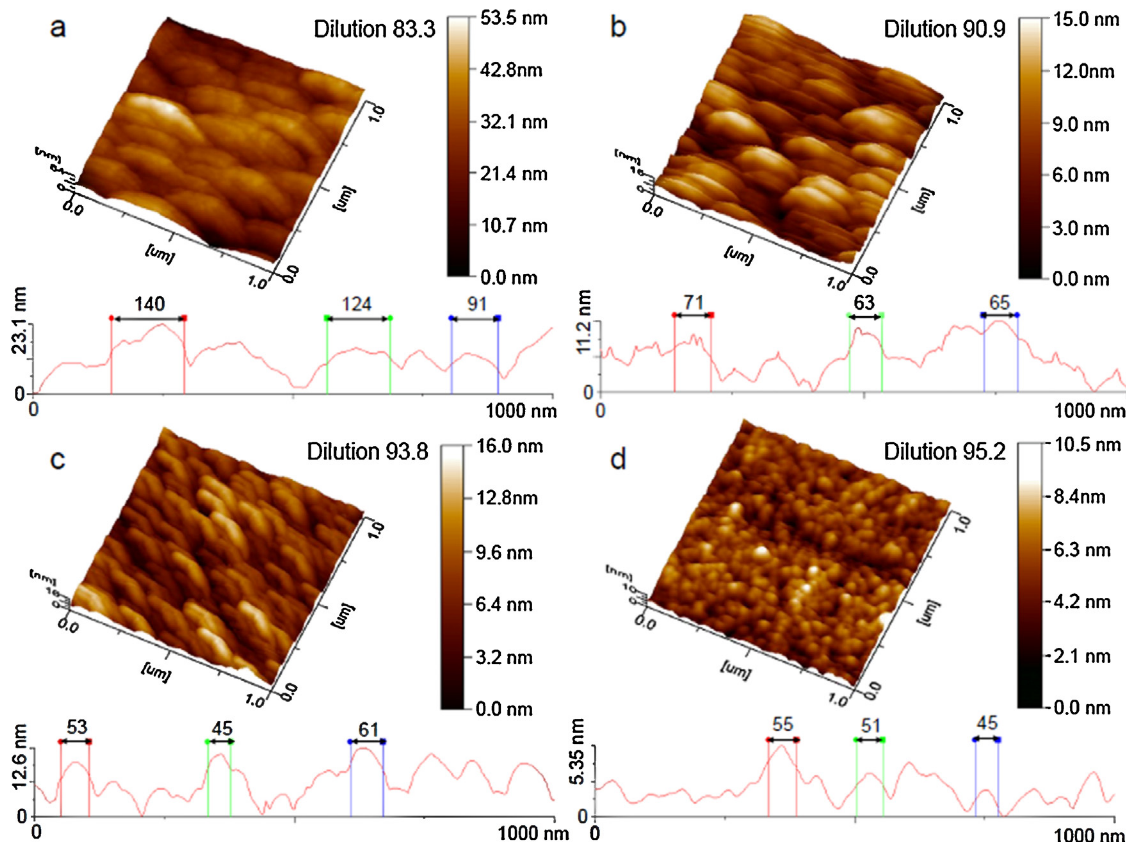

Fig. 3. 3D topography of pm-Si:H films grown by PECVD at 500 mTorr and dilution of: (a) 83.3, (b) 90.9, (c) 93.8 and (d) 95.2.

AFM. The little atomic percentage of chlorine in the films is due to chlorine extraction processes because the coexistence of H and Cl is chemically unstable in the growth surface and it is released spontaneously as HCl [2]. Our results show that Cl percentage decreases from 7% to 3% with increasing R_H, supporting this model. Also, increasing the deposition pressure to 500 mTorr has the same effect since the Cl percentage decreases to approximately one-half.

Fig. 8 shows high resolution XPS spectra of Si 2p peaks, taken at 15 min of erosion time for all samples used in this work. As a reference, lines are presented at the binding energies of 103.3 and 99.5 eV attributable to silicon dioxide (SiO_2) and elementary silicon, respectively. Binding energies of sub-stoichiometric oxidation states or Si—Cl bonds are expected to appear in between these references [28,32]. Fig. 8 shows different behaviors in Si 2p XPS spectra when both R_H and pressure are elevated. At 250 mTorr (Fig. 8a) when R_H is increased up to 93.8 only the peak corresponding to elementary Si is observed. At $R_H = 95.2$ a shoulder corresponding to SiO_2 becomes evident. Peak asymmetries can be related to SiO_x or Si—Cl bonds in the films. For the Si 2p XPS spectra at 500 mTorr (Fig. 8b) one can note that the samples with low R_H (83.3 and 90.9) present no evident oxidation. However, spectra corresponding to high R_H (93.8 and 95.2) present a peak at 103.3 eV indicating a prominent amount of oxidation.

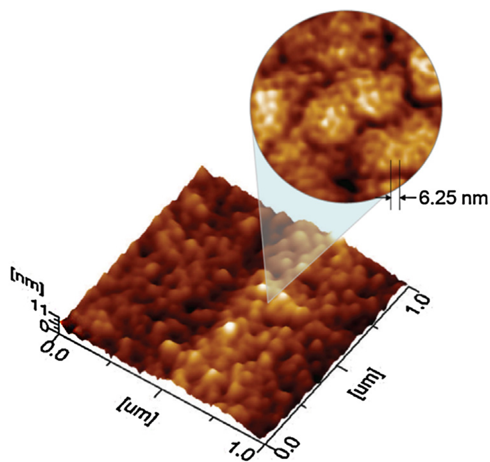

Fig. 4. 200 × 200 nm zoom area showing the film morphology corresponding to the sample grown with dilution of 95.2 at 500 mTorr. We can observe nanoparticles with size of about 6.25 nm that make up the cluster.

To investigate in further detail the chemical state of bonded silicon inside the film, we performed a deconvolution of the XPS spectra presented in Fig. 8. The results of this deconvolution are reported in Table 3 which includes the peak position in eV and its corresponding percentage of the total area. Representative examples of these deconvolutions are shown in Fig. 9. Peak 1 is associated with the presence of elementary silicon (position around 99.6 eV). An intermediary peak located around 100.6 eV is also observed in most samples. This peak has been associated with the Si^+ oxidation state [28,30–32]. In the case of our samples, this can be correlated to Si—Cl or Si—O bonds. For example, in Fig. 9 at low R_H only two peaks are observed associated to Si and Si^+. The area percentage corresponding to the Si^+ peaks is in correspondence with the amount of Cl and O presented in Fig. 6. This demonstrates that the low concentration of oxygen inside the films at low R_H is not present in the form of SiO_2. This incorporation of oxygen can be considered as structural defects of the silicon thin film, not enough in number to become a separate phase. On the other hand, for high R_H a third peak is present associated to higher Si oxidation states. This is consistent with the higher oxygen incorporation previously observed

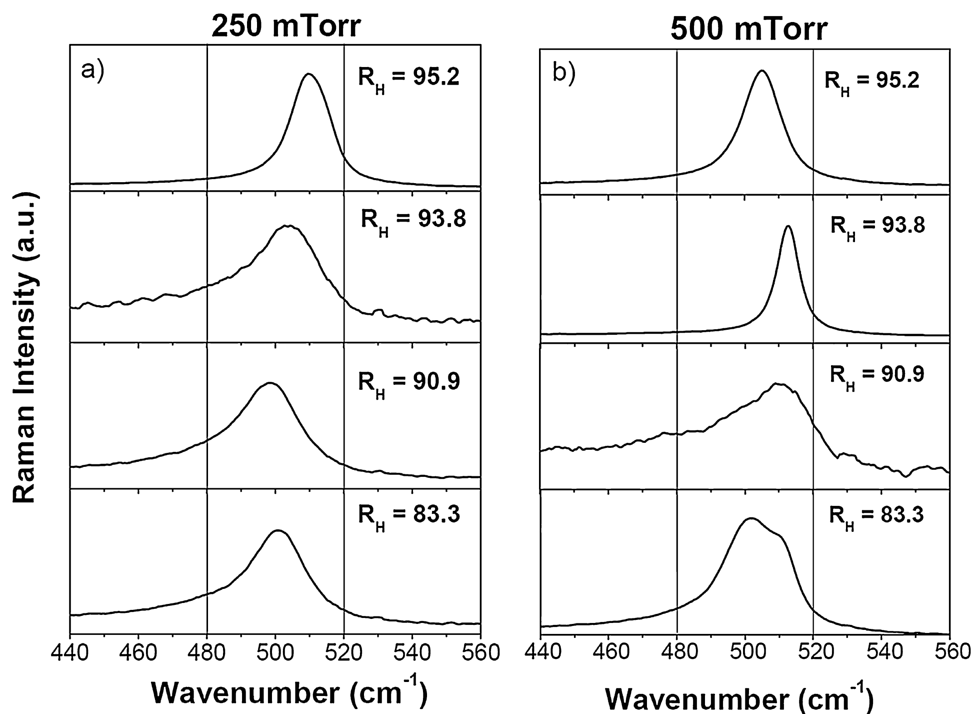

Fig. 5. Raman spectra of pm-Si:H thin films grown at (a) 250 mTorr and (b) 500 mTorr, with different hydrogen dilutions. Vertical lines show the positions of amorphous (480 cm^{-1}) and crystalline (520 cm^{-1}) phases.

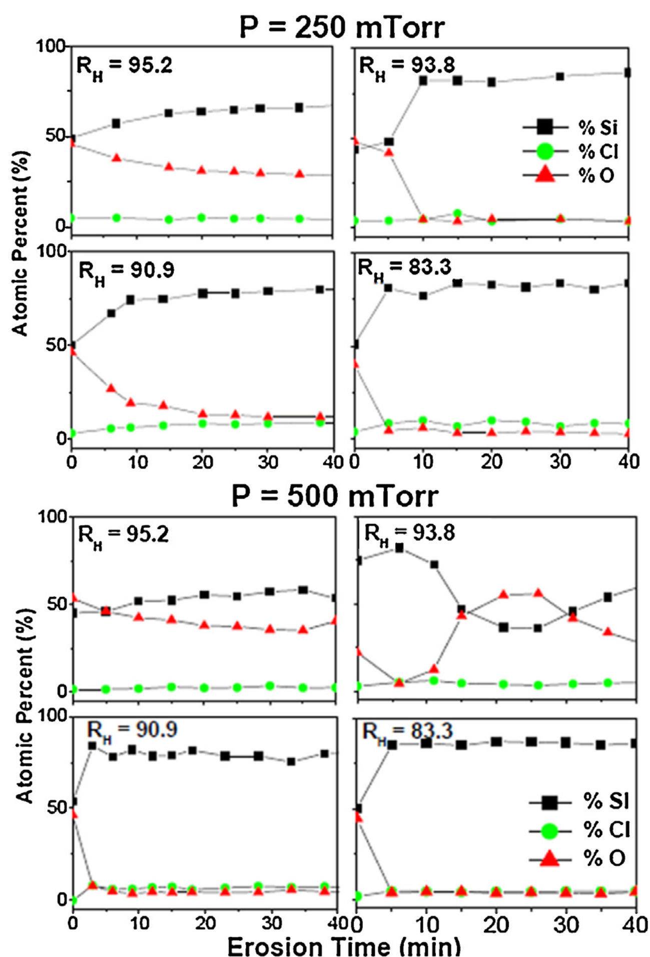

Fig. 6. Composition profiles of pm-Si:H thin films including atomic percents from Cl 2p, O 1s and Si 2p peaks for different argon ion erosion times.

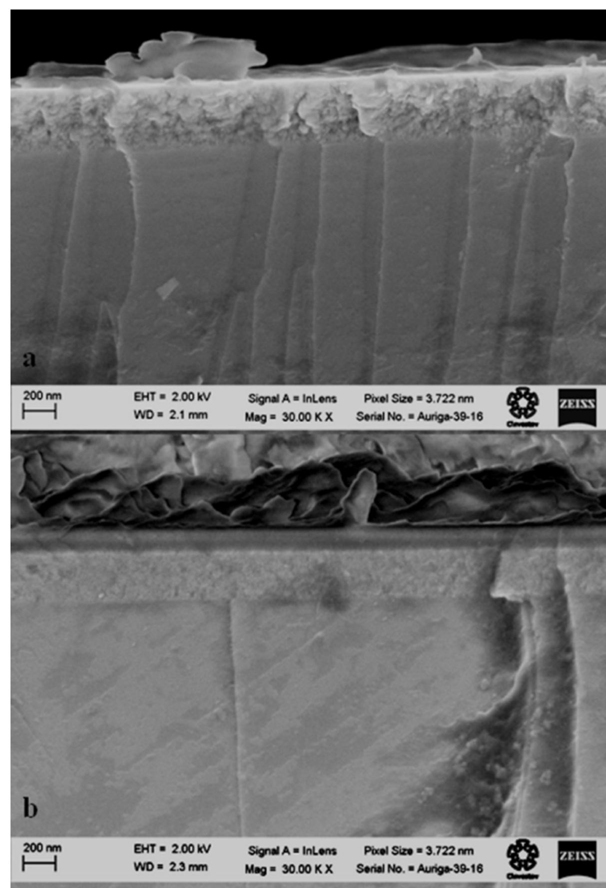

Fig. 7. Representative cross section SEM micrographs of porous oxidized films grown at (a) 250 mTorr with H_2 dilution of 95.2 and (b) 500 mTorr with H_2 dilution of 93.8.

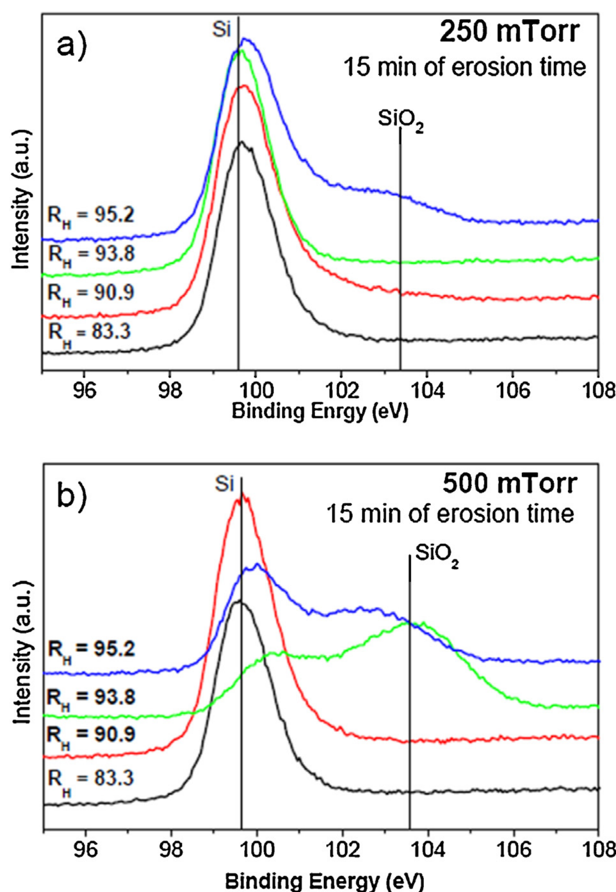

Fig. 8. Comparative XPS spectra of the Si 2p peak for the different hydrogen dilutions. The spectra were taken at 15 min of erosion time for the samples grown at (a) 250 mTorr and (b) 500 mTorr.

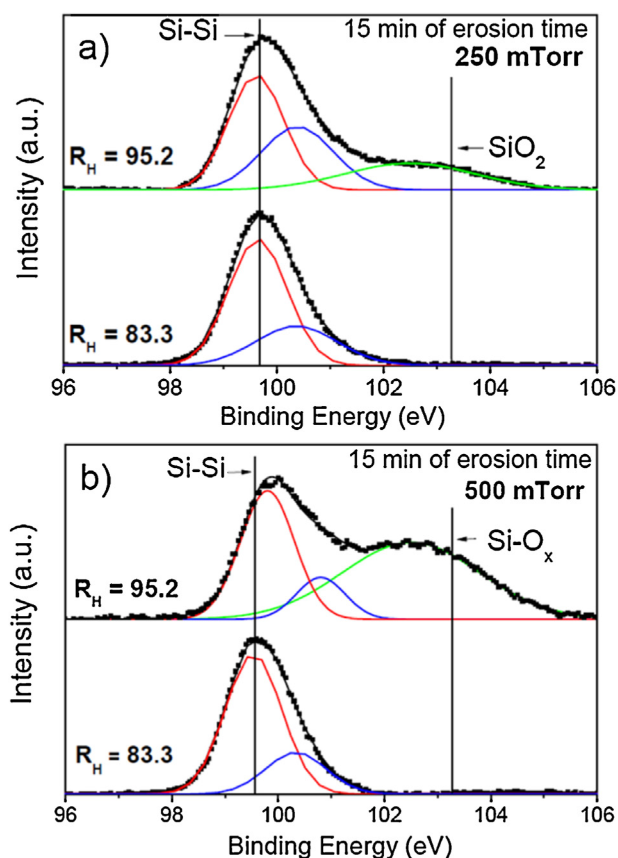

Fig. 9. Representative deconvolutions of the Si 2p peak for samples deposited at (a) 250 mTorr and (b) 500 mTorr for two different hydrogen dilutions.

in these films. It is noteworthy that the Si^{+} peak in these cases is much smaller corresponding mainly to Si—Cl.

XPS results have shown that growth regimes with low hydrogen dilution using dichorosilane as silicon precursor give as a result chemically stable films resistant to oxidation with a high degree of crystallization. High pressure and high hydrogen dilutions enhance the formation of substoichiometric oxides (SiO_x) due to ambient exposure which evidences the presence of a higher defect density and porosity of films grown under these conditions. These results were confirmed by cross section SEM micrographs.

3.4. Fourier transform infrared spectroscopy

FTIR results (Fig. 10) exhibit that the Si—H stretching mode around 1900–2100 cm^{-1} cannot be distinguished in our samples. This band is generally associated to silicon hydrides incorporated into the amorphous matrix [2–4,9,15,21,24,27] which are related with weak hydrogen bonds that are prone to generate light induced degradation of the material. Instead, the Si_mH_n wagging mode around 620–640 cm^{-1} is present in all cases. This mode has been correlated mainly with surface passivation of silicon nanocrystals in these type of pm-Si:H films [21,33,34]. Other bonding configurations corresponding to bending $(Si—H_2)_n$ modes are also present. On the other hand, as was observed previously by XPS, films deposited with high R_H present a considerable amount of oxidation evidenced by the prominent Si—O stretching band around 1070–1090 cm^{-1} [35]. This band is not evident for films deposited at low R_H, as expected from XPS results. Also, due to the small amount of incorporated chlorine in the films (less than 7 at.%), the stretching Si—Cl mode around 530 cm^{-1} cannot be distinguished in the FTIR spectra. From the perspective of application of these films as photovoltaic materials, having a high fraction crystalline in as grown films with low hydrides content in the amorphous matrix, is adequate for their utilization in silicon thin film solar cells.

Table 3
Peak center position (eV) and percentage of total area corresponding to the Si 2p XPS spectra deconvolution.

Sample R_H-pressure	Peak 1 position (eV)	Peak 2 position (eV)	Peak 3 position (eV)	Peak 1 area (%)	Peak 2 area (%)	Peak 3 area (%)
83.3–250	99.6	100.5	–	84	16	0
90.9–250	99.6	100.7	–	82	18	0
93.8–250	99.6	100.6	–	92	8	0
95.2–250	99.7	100.6	102.3	62	9	29
83.3–500	99.6	100.5	–	84	16	0
90.9–500	99.6	100.6	–	80	20	0
93.8–500	100.18	101.9	103.9	18	9	73
95.2–500	99.8	100.8	102.5	41	9	50

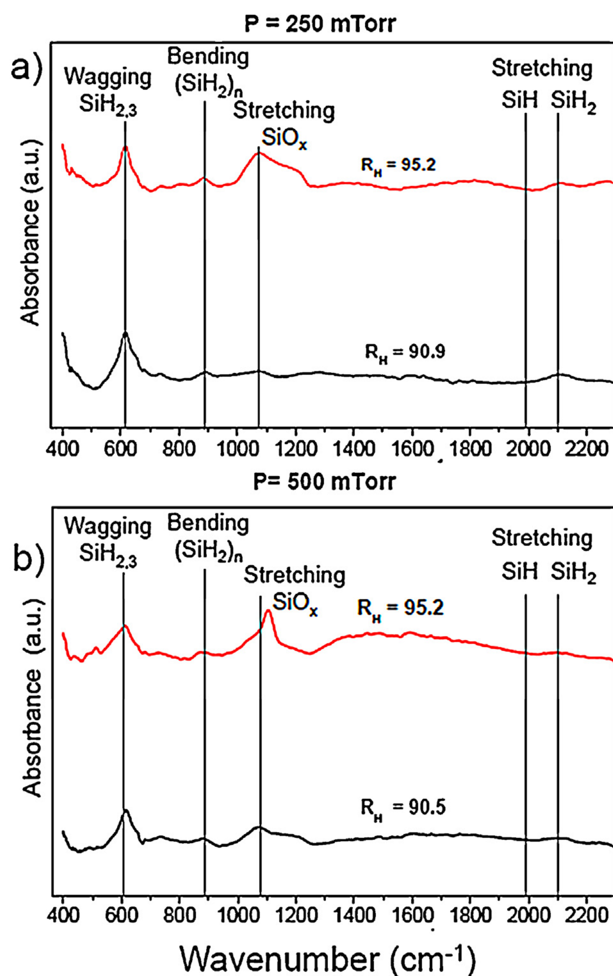

Fig. 10. Infrared spectra of pm-Si:H films deposited at (a) 250 mTorr and (b) 500 mTorr showing the absorbance peaks, for two different hydrogen dilutions.

4. Conclusions

The use of silicon chlorinated precursors enhances the crystallization process in as grown pm-Si:H samples, enabling the use of low hydrogen dilutions and pressures to obtain high crystallinity films. In contrast, for samples deposited with SiH_4, high plasma densities or high hydrogen dilutions are needed to obtain similar crystalline fractions. For the sample grown at 250 mTorr with the lowest hydrogen dilution, chlorine chemistry dominates the growth process generating a smooth surface with small clusters. Increasing hydrogen dilution causes plasma–surface interactions to become more prominent, increasing the density of nucleation sites and decreasing cluster height. At 500 mTorr, augmenting hydrogen dilution causes a considerable reduction in both roughness and topography, demonstrating an enhancement of ion bombardment and attack of the growing surface, which causes smaller growth rates. From the morphological analysis by AFM we can observe that the increase of ion bombardment has a direct influence on the amount of porosity and defects in the films. Also, an increase in atomic hydrogen interaction with the surface promotes crystallization through chlorine extraction as observed by Raman analysis.

XPS results show that the low concentration of oxygen inside the films grown at low R_H is present in the form of Si—O, which can be considered as structural defects. Instead, post-deposition oxidation increases with deposition pressure and dilution, due to film porosity, confirmed by cross section SEM analysis, generating a secondary SiO_x phase after ambient exposure. For higher pressure and dilution, the amount of chlorine incorporated to the film decreases congruently with HCl chlorine extraction processes involving atomic hydrogen interactions with the surface. In all cases, weak silicon hydride (Si—H) bonds were not detected by FTIR, while bonding configurations associated to the silicon nanocrystals surface were clearly observed. These results are very important because determining the differences in oxygen incorporation to the films after growth, along with chlorine and hydrogen, is fundamental in order to interpret the opto-electronic properties of these complex materials.

Acknowledgments

We acknowledge partial financial support for this work from DGAPA-UNAM PAPIIT Projects IN102411 and IB101612, CONACyT Mexico under project 153948 and ICyTDF project PICCO 10-73. The authors are grateful to Dr. J.C. Alonso and Dr. A. Ortiz† for the use of laboratory facilities and Dr. A. Remolina for samples preparation. A special acknowledgment is due to financial support from CONACyT through doctoral scholarship CVU 165872, SENER-CONACyT 151076, CONACyT 179632 and PAPIIT IN102411 thesis fellowships. Partial support from IPN with research project 20130293 is gratefully acknowledged. We also thank M.C. Josue Esau Romero Ibarra from Cinvestav-IPN for SEM characterization. Thanks are also due to J. Camacho, C. González and O. Jiménez for technical and information support.

References

[1] R. Butté, S. Vignoli, M. Meaudre, R. Meaudre, O. Marty, L. Saviot, P. Roca i Cabarrocas, J. Non-Cryst. Solids 266–269 (2000) 263–268.
[2] S. Jung, Y. Fujimura, T. Ito, H. Shirai, Sol. Energy Mater. Sol. Cells 74 (2002) 421–427.
[3] M.Y. Soro, M.E. Gueunier-Farret, J.P. Kleider, J. Appl. Phys. 109 (2011) 023713.
[4] L. Guo, J. Ding, J. Yang, G. Cheng, Z. Ling, N. Yuan, Appl. Surf. Sci. 257 (2011) 9840–9845.
[5] P. Roca i Cabarrocas, A. Fontcuberta i Morral, Y. Poissant, Thin Solid Films 403–404 (2002) 39–46.
[6] S.B. Li, Z.M. Wu, W. Li, Y.D. Jiang, N.M. Liao, Physica B 403 (2008) 2282–2287.
[7] M. Moreno, A. Torres, R. Ambrosio, C. Zuñiga, A. Torres-Rios, K. Monfil, P. Rosales, A. Itzmoyotl, Mater. Sci. Eng. B 176 (2011) 1373–1377.
[8] E.V. Johnson, L. Kroely, P. Roca i Cabarrocas, Sol. Energy Mater. Sol. Cells 93 (2009) 1904–1906.
[9] J. Kumar Saha, N. Ohse, K. Hamada, H. Matsui, T. Kobayashi, H. Jia, H. Shirai, Sol. Energy Mater. Sol. Cells 94 (2010) 524–530.
[10] L. Zhang, J.H. Gao, J.Q. Xiao, L.S. Wen, J. Gong, C. Sun, Appl. Surf. Sci. 258 (2012) 3221–3226.
[11] W. Beyer, in: N.H. Nickel (Ed.), Semiconductors and Semimetals, vol. 61, Academic Press, San Diego, 1999, p. 165.
[12] J. Fandiño, A. López-Suárez, B.M. Monroy, G. Santana, A. Ortiz, J.C. Alonso, A. Oliver, J. Electron. Mater. 35 (7) (2006) 1552–1557.
[13] P. Ho, W.G. Breiland, J. Appl. Phys. 63 (10) (1988) 5184.
[14] J. Nishizawa, K. Aoki, S. Suzuki, K. Kikuchi:, J. Cryst. Growth 99 (1990) 502–506.
[15] J.A. Yarmoff, D.K. Shuh, T.D. Durbin, C.W. Lo, D.A. Lapiano-Smith, F.R. MacFeely, F.J. Himpsel:, J. Vac. Sci. Technol. A 10 (1992) 2303–2307.
[16] T. Ito, K. Hashimoto, H. Shirai, Jpn. J. Appl. Phys. 42 (2003) L1119–L1122.
[17] H. Matsui, T. Saito, J.K. Saha, H. Shirai, J. Non-Cryst. Solids 354 (2008) 2483–2487.
[18] H. Shirai, T. Ito, Y. Ikeda, J. Non-Cryst. Solids 338–340 (2004) 115–118.
[19] B. Monroy, G. Santana, J. Aguilar Hernandez, A. Benami, J. Fandiño, A. Ponce, G. Contreras Puente, A. Ortiz, J.C. Alonso, J. Lumin. 121 (2006) 349–352.
[20] B.M. Monroy, G. Santana, A. Benami, A. Ortiz, J.C. Alonso, J. Fandiño, F. Cruz-Gandarilla, J. Aguilar-Hernández, G. Contreras-Puente, A. López-Suárez, A. Oliver, J. Nanosci. Nanotechnol. 9 (2009) 2902–2909.
[21] A. Remolina, B.M. Monroy, M.F. García-Sánchez, A. Ponce, M. Bizarro, J.C. Alonso, A. Ortiz, G. Santana, Nanotechnology 20 (2009) 245604.
[22] A. Remolina, L. Hamui, B.M. Monroy, M.F. García-Sánchez, A. Ponce, M. Picquart, G. Santana, Phys. Status Solidi C 8 (2011) 850–853.
[23] B.M. Monroy, A. Remolina, M.F. García-Sánchez, A. Ponce, M. Picquart, G. Santana, J. Nanomaterials 2011 (2011) 190632.
[24] S. Liu, X. Zeng, W. Peng, H. Xiao, W. Yao, X. Xie, C. Wang, Z. Wang, J. Non-Cryst. Solids 357 (2011) 121–125.
[25] V.S. Waman, M.M. Kamble, M.R. Pramod, S.P. Gore, A.M. Funde, R.R. Hawaldar, D.P. Amalnerkar, V.G. Sathe, S.W. Gosavi, S.R. Jadkar, J. Non-Cryst. Solids 357 (2011) 3616–3622.
[26] P. Dutta, S. Paul, D. Galipeau, V. Bommisetty, Thin Solid Films 518 (2010) 6811–6817.

[27] N. Budini, P.A. Rinaldi, J.A. Schmidt, R.D. Arce, R.H. Buitrago, Thin Solid Films 518 (2010) 5349–5354.
[28] S.G. Choi, H.-H. Park, J.-N. Jang, M. Hong, K.-H. Kwon, Ceram. Int. 38S (2012) S641–S644.
[29] Y. Sakuma, L. Haiping, H. Ueyama, H. Shirai, Vacuum 59 (2000) 266–276.
[30] K. Sato, T. Izumi, M. Iwase, Y. Show, H. Morisaki, T. Yaguchi, T. Kamino, Appl. Surf. Sci. 216 (2003) 376–381.
[31] C.K. Oh, S.D. Park, H.C. Lee, J.W. Bae, G.Y. Yeom, Electrochem. Solid-State Lett. 10 (2007) H94–H97.
[32] V.A. Terekhov, S.Y. Turishchev, K.N. Pankov, I.E. Zanin, E.P. Domashevskaya, D.I. Tetelbaum, A.N. Mikhailov, A.I. Belov, D.E. Nikolichev, S.Y. Zubkov, Surf. Interface Anal. 42 (2010) 891–896.
[33] H. Vach, Q. Brulin, N. Chaâbane, T. Novikova, P. Roca i Cabarrocas, B. Kalache, K. Hassouni, S. Botti, L. Reining, Comput. Mater. Sci. 35 (2006) 216–222.
[34] M. Kopáni, E. Pinčík, H. Kobayashi, M. Takahashi, N. Fujiwara, R. Brunner, M. Jergel, L. Ortega, Appl. Surf. Sci. 252 (2006) 7722–7725.
[35] V. Kapaklis, J. Non-Cryst. Solids 354 (2008) 612–617.